International Journal of Modern Physics B
Vol. 28, No. 12 (2014) 1442011 (25 pages)

DOI: 10.1142/S0217979214420119

World Scientific
www.worldscientific.com

Nonlinear pulse shaping and polarization dynamics in mode-locked fiber lasers

Sonia Boscolo*, Sergey V. Sergeyev, Chengbo Mou,
Veronika Tsatourian and Sergei Turitsyn

Aston Institute of Photonic Technologies,
School of Engineering and Applied Science,
Aston University, Birmingham B4 7ET, United Kingdom
**s.a.boscolo@aston.ac.uk*

Christophe Finot

Laboratoire Interdisciplinaire Carnot de Bourgogne,
UMR 6303 CNRS-Université de Bourgogne,
9 avenue Alain Savary, BP 47870, Dijon Cedex 21078, France

Vitaly Mikhailov, Bryan Rabin and Paul S. Westbrook

OFS Fitel, Somerset, New-Jersey, USA

Received 22 November 2013
Accepted 13 December 2013
Published 7 March 2014

We review our recent progress on the study of new nonlinear mechanisms of pulse shaping in passively mode-locked fiber lasers. These include a mode-locking regime featuring pulses with a triangular distribution of the intensity, and spectral compression arising from nonlinear pulse propagation. We also report on our recent experimental studies unveiling new types of vector solitons with processing states of polarization for multi-pulse and tightly bound-state soliton (soliton molecule) operations in a carbon nanotube (CNT) mode-locked fiber laser with anomalous dispersion cavity.

Keywords: Mode-locked fiber lasers; pulse shaping; pulse propagation and temporal solitons.

PACS numbers: 42.55.Wd, 42.65.Sf, 42.81.Dp, 42.81.Gs, 42.65.Re

1. Introduction

Passively mode-locked fiber lasers are now well developed and reliable devices used in a wide range of applications, including optical imaging and frequency metrology, material processing, telecommunications and biomedical research. While being very practical devices, mode-locked lasers are still very interesting objects for fundamental research in nonlinear science. From a fundamental standpoint, mode-locked fiber

lasers provide convenient and reproducible experimental settings for the study of a variety of nonlinear dynamical processes, thanks to the relative simplicity and precision of fiber-optic experiments. The complex interplay among the effects of gain/loss, dispersion and nonlinearity in a fiber cavity can be used to shape the pulses and manipulate and control the light dynamics and, hence, lead to different mode-locking regimes. This makes such lasers interesting realizations of so-called dissipative nonlinear systems.[1] Therefore, this research area is interesting in its own right. Classical short-pulse fiber oscillators are based on soliton formation in anomalous-dispersion cavities[2] or dispersion-managed (DM) solitons (stretched pulses) in cavities with a dispersion map.[3,4] Recently, new nonlinear mechanisms of pulse generation have been demonstrated in fiber lasers.[5] These include dissipative solitons in all-normal-dispersion cavities[6] and similaritons (pulses that evolve in a self-similar fashion have been dubbed similaritons) in passive[7] and active fibers.[8–12] Experimental interest in these nonlinear pulse-shaping regimes is strongly driven by the possibility of achieving pulse energy and peak power performances much higher than those of prior approaches and that can directly compete with solid-state systems. Despite substantial research in this field, qualitatively new phenomena are still being discovered. The interface between nonlinear science and laser physics is a promising area to transfer fundamental science knowledge to the design of very practical devices. In this paper, we review our recent results and advances in the area, by presenting a novel type of nonlinear pulse-shaping regime in a mode-locked fiber laser leading to the generation of linearly chirped pulses with a triangular temporal intensity profile,[13] and a new concept of a fiber laser architecture supporting self-similar pulse evolution in the gain fiber segment of the laser and nonlinear spectral pulse compression in a passive fiber.[14]

The vectorial nature of solitons has been recently explored beyond standard polarization locked states to reveal a rich spectrum of polarization dynamics in mode-locked fiber lasers.[15–20] Vector solitons in fiber lasers present a train of stabilized short pulses with the specific shape and state of polarization (SOP) defined by the interplay between the effect of anisotropy and the other conservative and dissipative effects in the laser cavity. The stability of vector solitons at different time scales from femtoseconds to microseconds is an important issue to be addressed for increased resolution in metrology,[21] spectroscopy[22] and suppressed phase noise in high-speed fiber optic communications.[23] In addition, there is a considerable interest in achieving high flexibility in generation and control of the dynamic SOPs in the context of trapping and manipulation of atoms and nanoparticles,[24,25] control of magnetization[26] and secure communications.[27] Recently, we have studied experimentally the conditions for emergence and suppression of vector solitons for fundamental, multi-pulse and bound-state soliton operations in a carbon nanotube (CNT) mode-locked fiber laser with anomalous-dispersion cavity.[19,20,28,29] In this paper, we overview our experimental results on the fast SOP evolution of multi-pulse vector solitons and tightly bound states — vector soliton molecules with fixed delay and phase differences. Among the aforementioned ap-

plications of controllable SOP dynamics, vector soliton molecules are of a special interest for telecommunication applications in the context of increased capacity in fiber optic communications based on polarization-division multiplexing, polarization switched and modified coded hybrid subcarrier/amplitude/phase/polarization modulation schemes.[30,31] Unlike the polarization dynamics of vector solitons on the Poincaré sphere demonstrated in Refs. 32 and 33, we unveil new insight into how polarization hole burning in an active medium contributes to the polarization dynamics. The observation of these new types of polarization dynamics was made possible by the development of a novel inline polarimeter optimized for high-speed operation.[29]

The paper is outlined as follows: Sec. 2 introduces the master model governing the optical pulse propagation in a fiber laser, and provides an overview of the recently discovered nonlinear mechanisms of pulse shaping in mode-locked fiber lasers along with the classical soliton and DM soliton mode-locking regimes. Section 3 discusses various methods to experimentally achieve passive mode locking that are extensively used and/or actively studied to generate ultra-short pulses in fiber lasers. Section 4 reports on our recent experimental observation of new types of multi-pulse and tightly bound-state vector solitons in a CNT mode-locked fiber laser. Finally, we conclude in Sec. 5.

2. Pulse Shaping

2.1. *Master model*

Pulse propagation in a fiber laser can be modeled with a modified nonlinear Schrödinger (NLS) equation that includes the dominant physical effects of the system — the master model pioneered by Haus.[34,35] These effects include group-velocity dispersion (GVD) and self-phase modulation (SPM) for all fibers, as well as gain saturation and bandwidth-limited gain for an active medium such as rare-earth doped fibers. The governing equations are given by

$$i\psi_z - \frac{1}{2}\beta_2\psi_{tt} + \gamma|\psi|^2\psi = \frac{i}{2}g\left(\psi + \frac{1}{\Omega^2}\psi_{tt}\right), \tag{1}$$

with the saturating gain

$$g = g(z) = \frac{g_0}{1 + W/W_0}\,. \tag{2}$$

Here $\psi = \psi(z,t)$ is the slowly-varying amplitude of the pulse envelope in a co-moving frame, β_2 is the GVD parameter and γ is the coefficient of cubic nonlinearity for the fiber section. Equation (1) differs from the well-known NLS equation due to the dissipative terms on the right-hand side of the equation, which represent linear gain, gain saturation and gain dispersion with a parabolic approximation to the gain profile with the bandwidth Ω. In Eq. (2), g_0 is the small-signal gain which is nonzero only for the gain fiber, $W(z) = \int \mathrm{d}t|\psi|^2$ is the pulse energy and W_0 is an

effective gain saturation energy corresponding to the saturation power (determined by the pump power) for a given repetition rate.

In addition to fiber propagation, the pulse experiences action induced by the discrete elements such as a saturable absorber, output coupler and spectral filter in mode-locked fiber lasers. Indeed, it is necessary to have some form of intensity discrimination to promote pulse formation from noise and to stabilize the pulse against perturbations as it traverses the cavity. Over the past two decades, a variety of different methods have been used to realize mode-locking pulse generation including, amongst others, nonlinear polarization rotation (NPR) which utilizes the Kerr effect of birefringent fiber as an artificial mode locker,[36,37] nonlinear interferometry,[2] semiconductor saturable absorber mirrors (SESAMs)[38,39] and more recently, carbon nanomaterials[40–44] which exploit nonlinear saturable optical absorption of the designated materials. Often, under certain conditions, the action of fast saturable absorbers can be approximated by a simplified, but generic, nonlinear transfer function[34]

$$\psi_f(t) = \left[1 - \frac{q_0}{1 + |\psi_i(t)|^2/P_0}\right]^{1/2} \psi_i(t)\,, \tag{3}$$

where ψ_i (ψ_f) is the input (output) field, q_0 is the unsaturated loss due to the absorber and P_0 is the saturation power. Note that this transfer function effectively promotes high intensities while attenuating lower intensities of the pulse. The discrete action of the output coupler can be approximated by a simple scalar multiplication of the field

$$\psi_f(t) = \sqrt{R} \times \psi_i(t)\,, \tag{4}$$

where we are assuming that any phase modulations caused are small, so that the laser output field would be given by $\sqrt{1-R} \times \psi_i(z,t)$. Finally, we consider the discrete action of a spectral filter $\hat{A}(\omega)$ on the pulse. The pulse form is modified in both amplitude and phase and can be written as

$$\psi_f(t) = \int_{-\infty}^{\infty} \mathrm{d}\omega \hat{\psi}_i(\omega) \times \hat{A}(\omega) e^{-i\omega t}\,, \tag{5}$$

where $\hat{\psi}(\omega)$ denotes the Fourier transform of $\psi(t)$. Including all effects of pulse propagation in passive and active fibers as well as the discrete elements of the saturable absorber, output coupler, and spectral filter allow for stable and robust mode-locking in a variety of experimentally realized configurations.[4,34,45]

2.2. *Soliton and dispersion-managed soliton mode locking*

Ultrashort pulses are stabilized in an oscillator when the effects of optical nonlinearity are exactly balanced by other processes after one cycle around the cavity. The most common way to compensate nonlinearity is through GVD. When the GVD

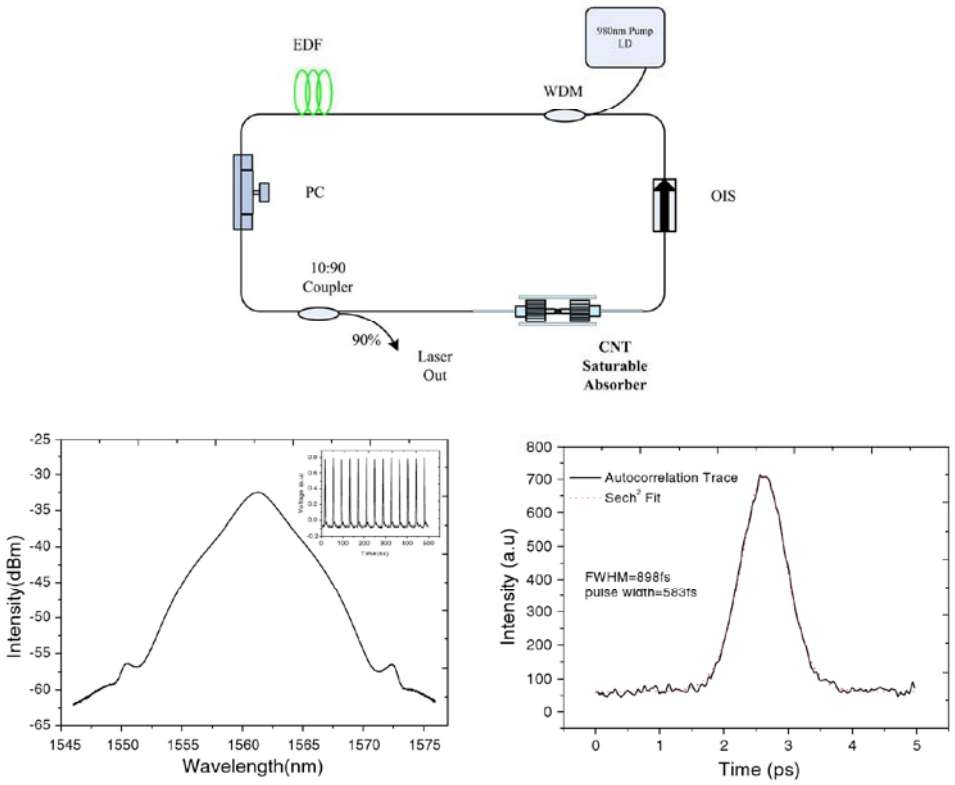

Fig. 1. Top: Schematic illustration of experimental anomalous-dispersion, CNT mode-locked fiber laser. EDF: erbium-doped fiber, PC: polarization controller, OIS: fiber pigtailed isolator, LD: laser diode, WDM: wavelength-division multiplexing. Bottom: Output optical spectrum, typical pulse train (inset) and measured autocorrelation trace of the output pulse. From Ref. 19.

is anomalous, pulses are formed by a balance between positive nonlinear and negative dispersive phase changes. The resulting soliton propagates indefinitely without change. Figure 1 illustrates the schematic configuration and the output of an all-fiber erbium-doped fiber laser with anomalous dispersion cavity and passively mode-locked with CNT polymer composite film.[19] The pronounced Kelly sidebands in the output optical spectrum centered at ~ 1560 nm indicate the fundamental soliton shape of the output pulses. The repetition rate of the output pulse train is $\sim$25.7 MHz and the fundamental soliton shape of $\mathrm{sech}^2(t/\tau)$ matches the measured autocorrelation trace with the pulse duration $\tau \sim 583$ fs. The average output power is ~ 3 mW corresponding to a pulse energy of $\sim$118 pJ.

While the soliton-like mode-locking regime is highly robust and the output pulse is transform limited, the pulse energy is limited to ~ 0.1 nJ in standard fiber by the soliton area theorem, $W\tau \propto \beta_2/n_2$, which expresses the nonlinear and dispersive phase shift balance (n_2 is the nonlinear index of the fiber). The combination of solitons and chirped pulses allows for higher pulse energies because a chirped pulse

has more energy than a transform-limited pulse of equal peak power and nonlinear phase accumulation. In a laser with segments of large and nearly equal magnitudes of GVD but with opposite signs (referred to as a dispersion map), a pulse will stretch and compress and the nonlinear phase is exactly balanced by the net effect of dispersion. These stretched-pulse fiber lasers[3] implement the concept of dispersion management of solitons that has been also studied in optical communications,[4,45–48] and support the analog of DM solitons. The DM soliton operation exists for net anomalous or small normal GVD and allows pulse energies an order of magnitude larger than the ordinary soliton operation. Recent theoretical and experimental work[6,49] has shown that much higher pulse energies can be achieved in fiber lasers that operate at normal dispersion. In the normal dispersion regime solitons do not form, so new pulse-shaping processes are needed. In the following sections, we will review some of these pulse-shaping processes and pulse evolutions.

2.3. *Parabolic self-similar and triangular pulse evolutions*

Pulses that propagate in normal-dispersion media are susceptible to distortion and breakup owing to optical wave breaking,[50] which is a consequence of excessive nonlinear phase accumulation combined with dispersion. In 1993 Anderson *et al.* showed that a sufficient condition to avoid wave breaking is that a pulse acquires a monotonic instantaneous frequency shift or chirp as it propagates, and that wave-breaking-free solutions of the NLS equation exist when the GVD is normal.[51] These are asymptotic solutions of the NLS equation in the quasi-classical or WKB limit (i.e., the limit of high amplitude or small dispersion), and take the form

$$|\psi(z,t)| = a(z)\sqrt{1-(t/\tau(z))^2}\,\theta(\tau(z)-|t|)\,, \quad \arg\psi(z,t) = b(z)t^2 + \phi_0(z) \qquad (6)$$

and thus have parabolic intensity profiles. Here, $\theta(x)$ is the Heaviside function. Such a pulse maintains its shape and is always a scaled version of itself (Fig. 2); i.e., it evolves self-similarly. In contrast to solitons or DM solitons, self-similar pulses can tolerate strong nonlinearity ($\phi^{\mathrm{NL}} = \int \mathrm{d}z\gamma(z)P_0(z) \gg 1$, where ϕ^{NL} is the peak nonlinear phase shift and P_0 the pulse peak power) without distortion or wave breaking. The normal GVD effectively linearizes the accumulated phase of the pulse allowing for the spectral bandwidth to increase without destabilizing the pulse. Similaritons were later demonstrated theoretically and experimentally in single-pass fiber amplifiers,[52,53] and they continue to attract much attention.[54] Self-similar pulses in fiber amplifiers are, along with solitons in passive fiber the most well-known classes of nonlinear attractors for pulse propagation in optical fiber, so they take on major fundamental importance.

Considering the stringent limitations to the energy of short pulses in fiber lasers, the possibility of exploiting self-similar propagation in a laser is very attractive. The design of a laser that will support self-similar pulse evolution must address two key issues. Firstly, self-similar pulses evolve monotonically, and such evolution is incompatible with the periodic boundary condition of a laser; mechanism(s) must

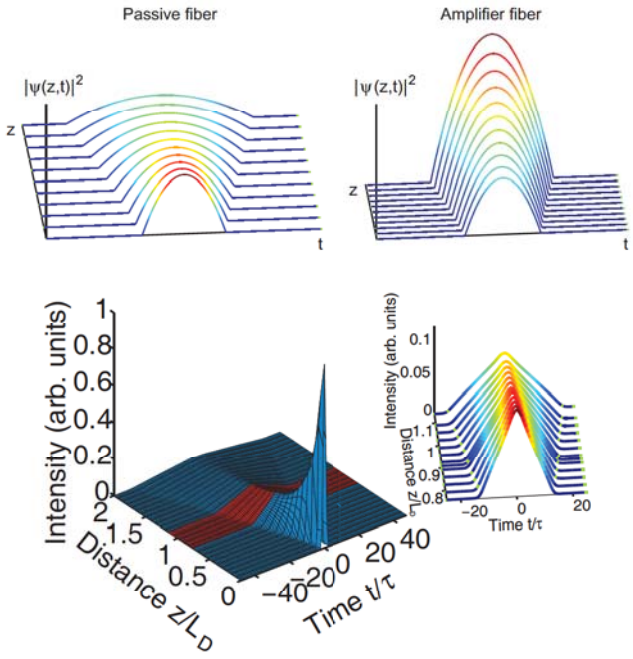

Fig. 2. Top: Illustration of self-similar evolution in ordinary fiber or amplifier fiber. Bottom: Evolution of an initial Gaussian pulse toward a triangular pulse in ordinary fiber (τ is a temporal characteristic value of the initial pulse and $L_{\mathrm{D}} = \tau^2/|\beta_2|$ is the dispersion length). The pulse profiles over the life distance of the triangular solution are shown in the inset. Adapted from Ref. 13.

be provided to reverse any changes and thus restore the solution after traversal of the cavity. Second, self-similar evolution is disrupted if the pulse encounters a limitation to its bandwidth. This must be reconciled with the tendency of a pulse to fill available gain bandwidth. The approach taken by Ilday *et al.*[7] was to design a laser that would support self-similar evolution in a passive fiber segment which are subsequently amplified in the presence of minimal dispersion and nonlinearity. The laser shown schematically in Fig. 3 addresses these issues. A short segment of gain fiber decouples gain filtering from the nonlinear evolution in the long segment of passive fiber, and the chirp accumulated in the passive fiber is compensated by linear, anomalously dispersive delay.

We have recently shown theoretically that in the normal-dispersion regime of a passive fiber, starting from a conventional field distribution, e.g., from a Gaussian pulse, aside from parabolic waveforms it is possible to generate other advanced field distributions such as flat-top- and triangular-profiled pulses with a linear frequency chirp.[55] Such pulse waveforms represent transient states of the nonlinear pulse evolution in the fiber medium and can be associated with an intermediate asymptotic regime[56] of the pulse propagation. As such, they have a finite life distance (characteristic length scale of the self-similar pulse dynamics) that depends

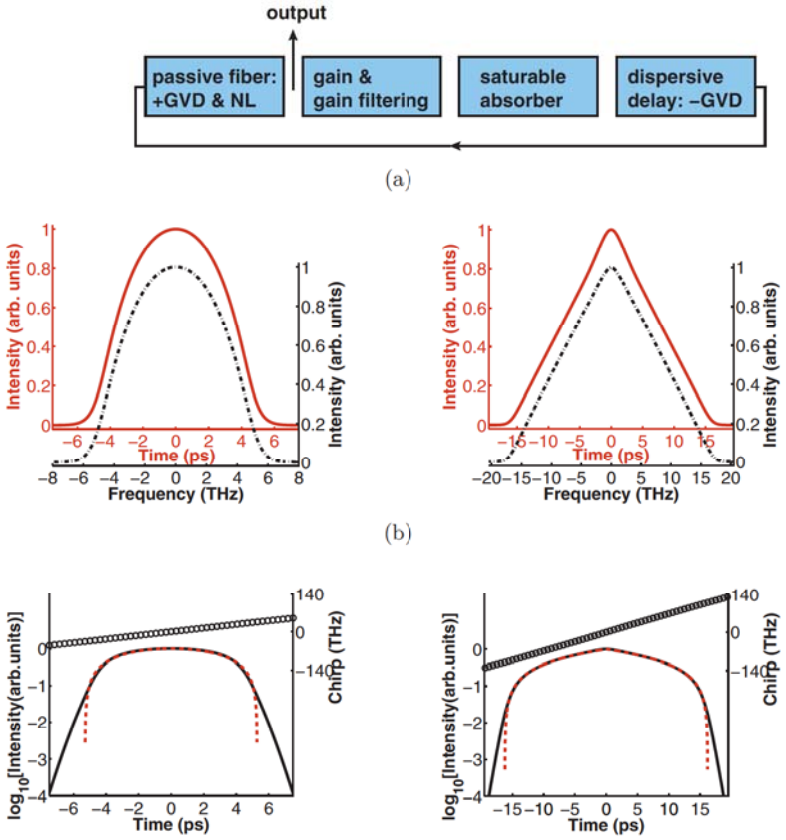

Fig. 3. (Color online) Top: Schematic of a conceptual laser that supports parabolic self-similar and triangular pulse formation. Bottom: Pulse solutions in the parabolic (left) and triangular (right) pulse-shaping regimes: (a) Temporal (solid red) and spectral (dash-dotted black) intensity profiles of the pulse at the end of the passive fiber. (b) Temporal profiles on a log scale (solid black) and chirp profiles (open black circles). The corresponding parabolic and triangular fits are also shown (dashed red). Adapted from Ref. 13.

on the initial conditions. An example of the evolution of an initial Gaussian pulse toward a pulse with a triangular intensity profile is presented in the right panel of Fig. 2. These theoretical results have been confirmed experimentally by intensity and phase measurements of the generated pulses.[57]

In Ref. 13, we have exploited intermediate asymptotic evolution in a practical laser system. We have numerically demonstrated the possibility of pulse shaping in a mode-locked fiber laser using control of the intra-cavity propagation dynamics by adjustment of the normal net dispersion and integrated gain of the cavity. Using a laser cavity similar to that described in Ref. 7 (Fig. 3), the existence of two distinct steady-state solutions of stable single pulses in different regions of the system parameter space has been shown: the previously known parabolic self-similar pulse and a pulse with a triangular waveform and a linear chirp. Parabolic-shaped

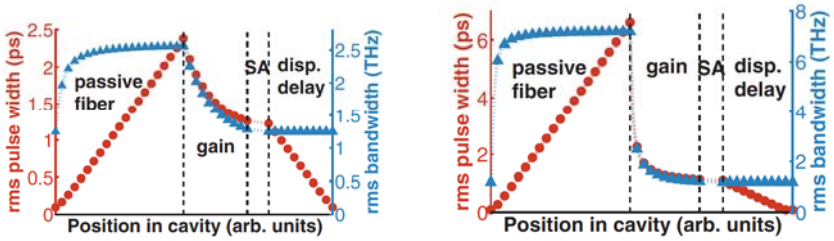

Fig. 4. (Color online) Evolution of the rms temporal (red circles) and spectral (blue triangles) widths along the cavity in the parabolic (left) and triangular (right) pulse-shaping regimes. Adapted from Ref. 13.

pulses were obtained for relatively large values of the net dispersion and moderate gain values. In contrast, triangular-shaped pulses were observed for smaller net dispersion and rather high gain values. Solutions obtained at representative points in the parameter space of the parabolic and triangular pulse regimes are shown in the bottom panel of Fig. 3. The pulse evolution is illustrated by plots of the root-mean-square (rms) pulse duration and spectral bandwidth as functions of position in the cavity (Fig. 4). For the parabolic pulse regime, the parabolic temporal profile after the passive fiber, linear frequency chirp and imaging of the temporal shape in the spectral domain are all signatures of what is well known from self-similar propagation and mode-locking[7] and are due to self-similar evolution in the fiber. The nonlinear evolution in the passive fiber is monotonic with the growth of both temporal and spectral widths. The generated bandwidth is filtered by the gain medium, and the pulse is always positively (normally) chirped inside the cavity.[7] In the case of triangular pulse shaping, pulses with both triangular temporal and spectral intensity profiles are obtained after the passive fiber. The spectral shape reflecting the temporal shape is again a result of the linear chirp and high value of the chirp coefficient. This can be explained using the stationary phase method, i.e., the cancelation of oscillating contributions with rapidly varying phase in the Fourier transform integral. Similarly to the parabolic pulse regime, the nonlinear evolution in the passive fiber is monotonic, though the scales of temporal and spectral broadening are larger. The main difference from the parabolic regime is that the chirp is changed from positive at the end of the gain fiber to negative (anomalous) at the entrance of the passive fiber by the dispersive delay, and correspondingly, the pulse compresses to minimum duration in the dispersive-delay element. The anomalous chirp at the entrance of the passive fiber is consistent with our findings on triangular pulse generation in single-pass fiber systems.[55,57]

2.4. *Amplifier similariton mode locking and nonlinear spectral compression*

Because the spectral bandwidth of the pulse increases substantially in self-similar amplification, the formation of a self-consistent solution in a laser cavity which

would support self-similar evolution in the gain fiber segment of the cavity requires the compensation of spectral broadening. Parabolic amplifier similaritons were recently stabilized in an oscillator.[8,10,12] Spectral filtering was found to play a critical supporting role to stabilizing the amplifier similaritons in the cavity. Unlike the passive similariton regime, the amplifier similariton laser relies on a local nonlinear attraction to stabilize the pulse. An arbitrary pulse inserted into a gain fiber is nonlinearly attracted to an asymptotically evolving parabolic pulse. The output pulse parameters are entirely determined by the energy of the input pulse and the parameters of the fiber. This nonlinear attraction entails pulse's independence from the global cavity parameters. Shorter, nearly transform-limited pulses can reach the amplifier similariton solution in shorter propagation lengths.[52] Oktem *et al.* built a laser where the parabolic pulse, following spectral filtering, gradually evolves into a soliton in an anomalous-dispersion segment, which allows for a short transform-limited pulse to return to the input of the gain fiber.[8] In the all-normal-dispersion laser demonstrated by Renninger *et al.*,[10] strong spectral filtering compensates both the broad pulse duration and bandwidth after the gain segment and, hence, facilitates the creation of a self-consistent cavity. Indeed, for fixed chirp, a pulse with a narrower spectrum is shorter and closer to the transform limit. However, such filtering introduces high energy loss. Aguergaray *et al.* built a Raman oscillator with kilometers of gain fiber, which provides enough propagation length for the asymptotic solution to be achieved.[12]

We have recently proposed a new concept of a fiber laser architecture that supports self-similar pulse evolution in the amplifier and nonlinear spectral pulse compression in the passive fiber.[14] In this design (Fig. 5), a dispersive-delay line which supplies anomalous GVD with negligible nonlinearity, imparts a negative frequency chirp onto the positively chirped pulse as produced by the fiber amplifier. The negatively chirped, large-bandwidth pulse is then spectrally compressed in a normally dispersive fiber. Indeed, the frequency chirp induced by SPM in the fiber (equaling minus the first derivative of the intensity-dependent nonlinear phase shift) brings a frequency downshift of the leading edge and an upshift of the trailing edge

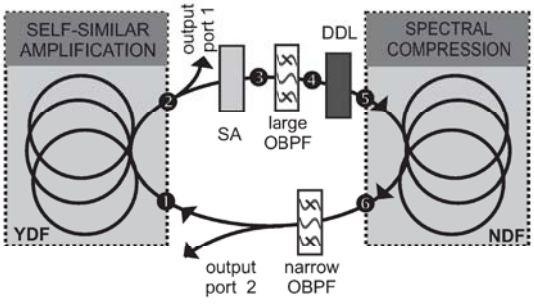

Fig. 5. Schematic of a laser designed to support self-similar pulse amplification and nonlinear spectral compression. From Ref. 14.

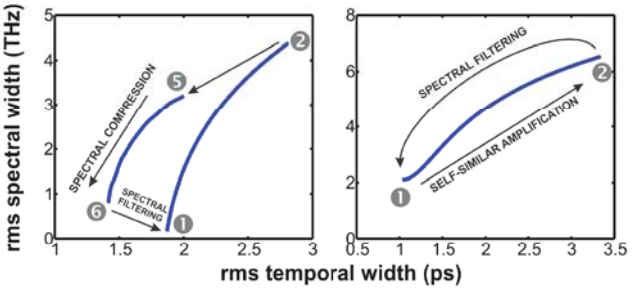

Fig. 6. Phase diagram representing the combined evolution of the rms temporal and spectral widths of the pulse over one roundtrip in the cavity with (left) and without (right) nonlinear spectral compression. From Ref. 14.

of the pulse, i.e., a positive chirp. Consequently, for a negatively chirped input pulse the linear and nonlinear phases cancel each other, leading to a redistribution of long and short wavelengths toward the center wavelength and therefore to spectral compression instead of spectral broadening.[58] This results in a significant increase of the energy spectral density. This spectral compression process is the key feature of our laser setup. A large spectral filter after the gain fiber and saturable absorber improves the stability of the laser, and a narrow filter is used after the passive fiber (only) to suppress the spectral wings due to imperfect compression.

The intra-cavity pulse evolution is illustrated in Fig. 6. Also shown is the evolution in an amplifier similariton fiber laser consisting of a gain segment, a saturable absorber, and a spectral filter.[10] The pulse solution at different locations within the cavity is shown in Fig. 7. The pulse duration and bandwidth increase monotonically in the gain fiber as the pulse evolves toward the asymptotic attracting solution in the fiber. The resultant pulse after the gain segment is highly parabolic, and the associated spectrum exhibits some structure, as expected for a parabola with finite (though large) chirp (Fig. 7). Cancelation of the highly linear chirp outside the laser cavity can lead to high-quality temporally compressed pulses with high energies. In the similariton laser, the main pulse shaping mechanism relies on the attracting nature of amplifier similaritons, which is then compensated by strong spectral filtering (Fig. 6). In contrast, the pulse-shaping mechanism of our laser design is dominated by two nonlinear processes with distinctly different dynamics: similariton formation with nonlinear attraction in the gain fiber, and spectral compression arising from nonlinear propagation in the passive fiber and leading to large spectral narrowing. The first large filter carves the output spectrum from the amplifier, and the linear dispersive delay only affects the temporal width of the pulse. The spectral width of the pulse at the output of the passive fiber is comparable to the bandwidth of the narrow filter (Fig. 7). The energy spectral density of the pulse is therefore largely increased, and nonlinear spectral compression benefits the laser's power efficiency by preventing strong spectral filtering from being highly dissipative. Further, the direct generation of transform-limited picosecond pulses from the laser is made possible.

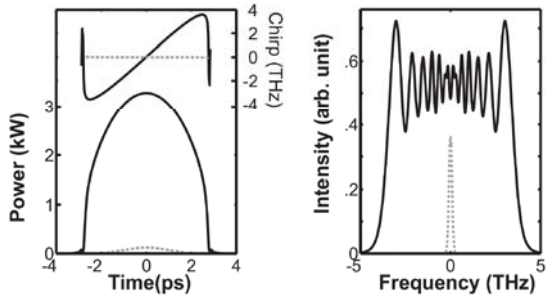

(a)

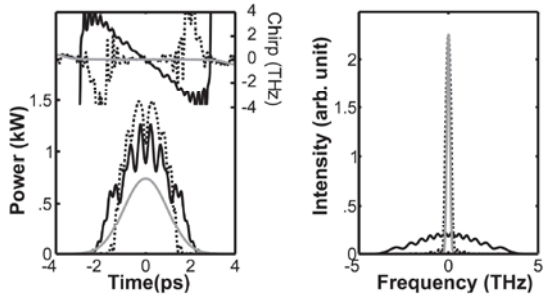

(b)

Fig. 7. Temporal intensity and chirp profiles (left) and spectral intensity profiles (right) of the pulse at (a) the entrance (dotted) and the exit (solid) of the gain fiber, and (b) the entrance of the passive fiber (solid black), the end of the passive fiber (dotted black), and after the narrow spectral filter (solid grey). From Ref. 14.

The output pulse from the spectral compression port exhibits a transform-limited picosecond temporal profile with a time-bandwidth product nearly equalizing the transform limit for a Gaussian pulse (0.441). Note that in the amplifier similariton laser the pulse after spectral filtering is still chirped and far from being transform limited. By varying the length of the passive fiber, period-doubling bifurcations[59] and chaotic pulse dynamics were also observed in the system.

3. Mode-Locking Techniques

As mentioned in the previous section, pulse shaping in mode-locked fiber lasers strongly relies on the mechanisms of mode locking. Passive mode locking offers a neat approach to generate short pulses. To passively mode-lock a laser, an intensity discrimination mechanism is necessary, or the so-called mode locker or saturable absorber. For artificial saturable absorbers, such as those based on NPR[36,37] and nonlinear interferometry,[2] nonlinear effects play a crucial role, while for physical saturable absorbers, such as SESAMs,[38,39] CNTs[40,41] and graphene,[44] the material properties dominate the field. In this section we discuss some of these mode-locking techniques and their implementations in fiber lasers.

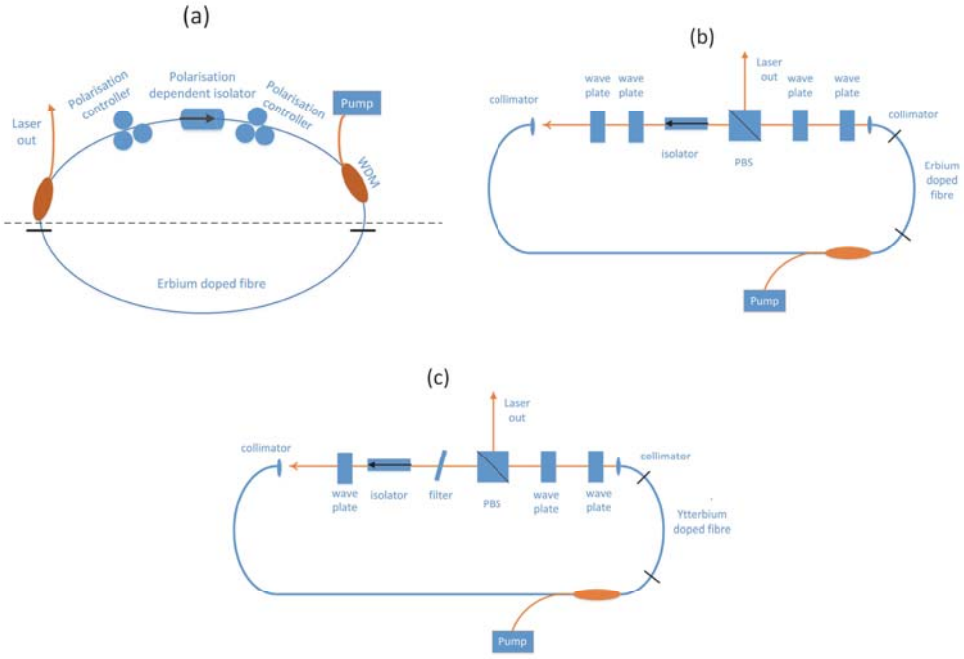

Fig. 8. Schematic configuration of (a) a conventional soliton fiber laser using a fiber polarizer, (b) a high-energy stretched-pulse fiber laser, and (c) a dissipative soliton fiber laser with a spectral filter.

3.1. *Nonlinear polarization rotation*

3.1.1. *Polarizer based mode locking*

So far NPR has proved to be the most effective way to generate different types of pulses in fiber lasers. By using a polarizer and wave plates (polarization controllers) and with proper cavity designs, mode-locked fiber lasers with various pulse regimes have been achieved. A conventional soliton fiber laser configuration is shown in Fig. 8(a).[36] If the erbium-doped fiber has normal GVD, the rest of the cavity consists of a fiber with anomalous GVD (SMF28). When the overall dispersion is negative, the laser operates in the classical soliton regime with typical Kelly side bands in the optical spectrum. Higher pulse energies and shorter pulses can be achieved with a stretched-pulse laser cavity,[3] which uses a longer erbium-doped fiber segment and a shorter segment of SMF28 to maintain the net cavity dispersion around zero. A widely applied technique to maximize the output pulse energy is to output light from the cavity by means of a bulk polarizer rather than a coupler [Fig. 8(b)]. The dissipative soliton regime has been recently demonstrated, using a spectral filter in an ytterbium-based fiber laser for high-energy pulse shaping [Fig. 8(c)].[6] The development of such a system has also led to the similariton fiber laser.[7–10]

3.1.2. *Tilted fiber grating based mode locking*

In addition to the high energy output, the all-fiber format of mode-locked fiber lasers also attracts much attention due to its inherent compact design and intrinsic compatibility to the telecom fiber-optic systems. As an in-fiber device, fiber Bragg gratings[60,61] have been studied extensively over the past few decades. They have found very wide applications as filters, mirrors, dispersion compensators and sensors. Various types of fiber gratings have been developed to further enhance the capabilities of standard fiber Bragg gratings, such as phase-shifted,[62] long-period,[63] sampled[64] and tilted[65] gratings. Among these, tilted fiber gratings (TFGs) represent a novel type of in-fiber devices with attractive core/cladding/radiation mode coupling characteristics. Recently, a special type of an TFG with strong polarization-

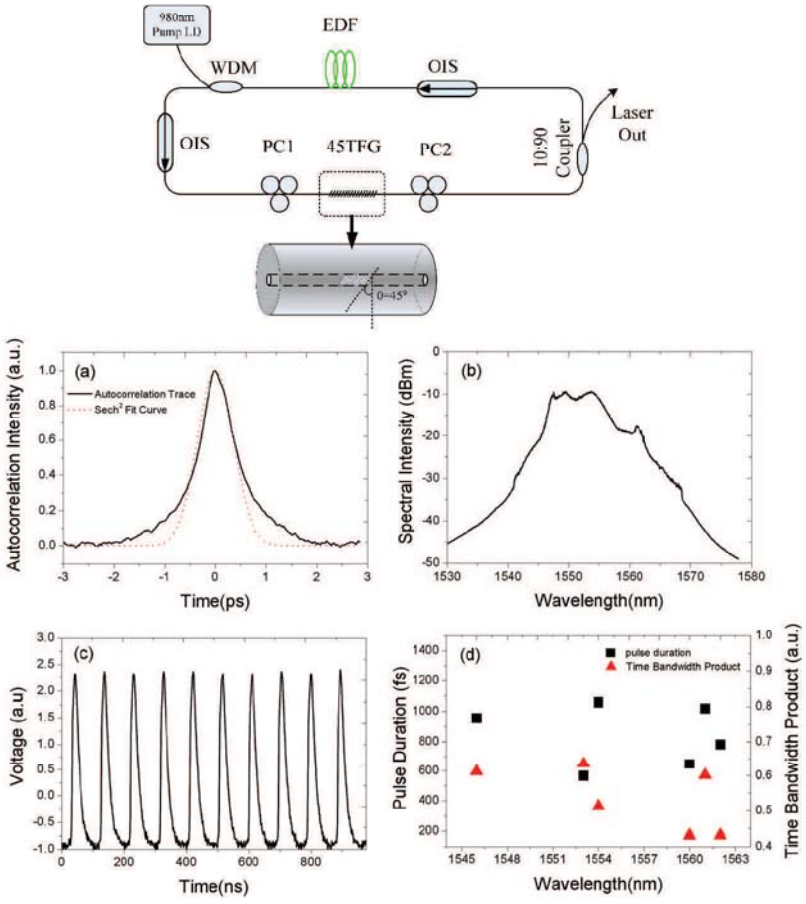

Fig. 9. Top: Schematic configuration of a 45°-TFG based mode-locked soliton fiber laser. Bottom: (a) Measured auto-correlation trace and corresponding sech^2 fit, (b) optical spectrum of the output pulse, (c) typical output pulse train and (d) measured pulse width and time-bandwidth products as a function of the wavelength. Adapted from Ref. 66.

dependent loss properties, the 45°-TFG, has been shown to be an efficient tool for pulse shaping in mode-locked fiber lasers.[66–69] Such polarizer is based on the pile-of-plate principle which taps out the s-light and propagates the p-light, and benefits from the all-fiber structure and low insertion loss.[70,71] The cost of such gratings could also be low as they can be produced using standard UV inscription in conventional telecom fibers (SMF28). Details of the fabrication and characterization of the 45°-TFGs used in our experiment can be found in Refs. 66 and 69. The top panel of Fig. 9 shows the schematic configuration of an all-fiber femtosecond erbium-doped fiber laser passively mode-locked using a 45°-TFG as an in-fiber polarizer in the laser cavity.[66] The laser consists of ~ 6 m commercial erbium-doped fiber with normal GVD. The rest of the cavity consists of 12 m SMF28 and a 50 cm B/Ge fiber, incorporating the 45°-TFG, with anomalous GVD. The net-anomalous dispersion of the laser cavity is $\sim +8.5$ ps/nm/km. Two polarization-independent isolators (OIS) are used to maintain single-direction oscillation of the laser. The fiber laser is pumped through a 980/1550 wavelength-division multiplexing (WDM) from a 975 nm laser diode, which can provide up to 300 mW pump power. A commercial laser diode driver and controller are used for stabilizing the pump diode. Two fiber paddle-based polarization controllers (PC1 & PC2) are located before and after the 45°-TFG. A 10:90 fiber coupler is employed to couple out 10% the laser light. The effect of NPR with the 45°-TFG based inline polarizer provides the necessary intensity discrimination for mode locking. Since the net GVD is anomalous, GVD and SPM counterbalance to give soliton-like pulses. By properly adjusting the two polarization controllers in the system, stable mode-locked pulses can be obtained. The bottom panel of Fig. 9 shows the measured auto-correlation trace of the $\sim$ 600 fs output pulse and the optical spectrum of the pulse centered at 1553 nm with a spectral bandwidth at full-width half-maximum of ~ 9 nm, thus giving a time-bandwidth product of ~ 0.6, indicating the pulse is slightly chirped. A typical pulse train is also shown with a 90 ns interval between two adjacent pulses, giving a repetition rate of 10.34 MHz. The output pulse power is 12 mW which corresponds to the output energy of ~ 1 nJ, which is ~ 10 times that of typical soliton mode-locked lasers. By adjusting the two sets of polarization controllers, the mode-locked wavelength exhibits a certain degree of tunability from 1548 nm to 1562 nm with pulse durations from $\sim$ 600 fs to ~ 1 ps. The measured pulse width and time-bandwidth product as a function of the wavelength also demonstrate the tunability of the fiber laser. Since the time-bandwidth product of the output pulses is larger than 0.315, the output pulses are not transform limited. However, simple optimization of the cavity design could achieve transform-limited pulses at the output coupler.

Very recently, we have also used the polarization functionality of a 45°-TFG in an NPR mode-locked erbium-doped fiber laser operating in a dissipative stretched-pulse regime shown in Fig. 10.[69] The laser cavity has a net GVD of $+0.013$ ps^2 and outputs pulses with sub-100 fs duration and 1.68 nJ energy. To the best of our knowledge, this is the shortest pulse generated from mode-locked lasers with

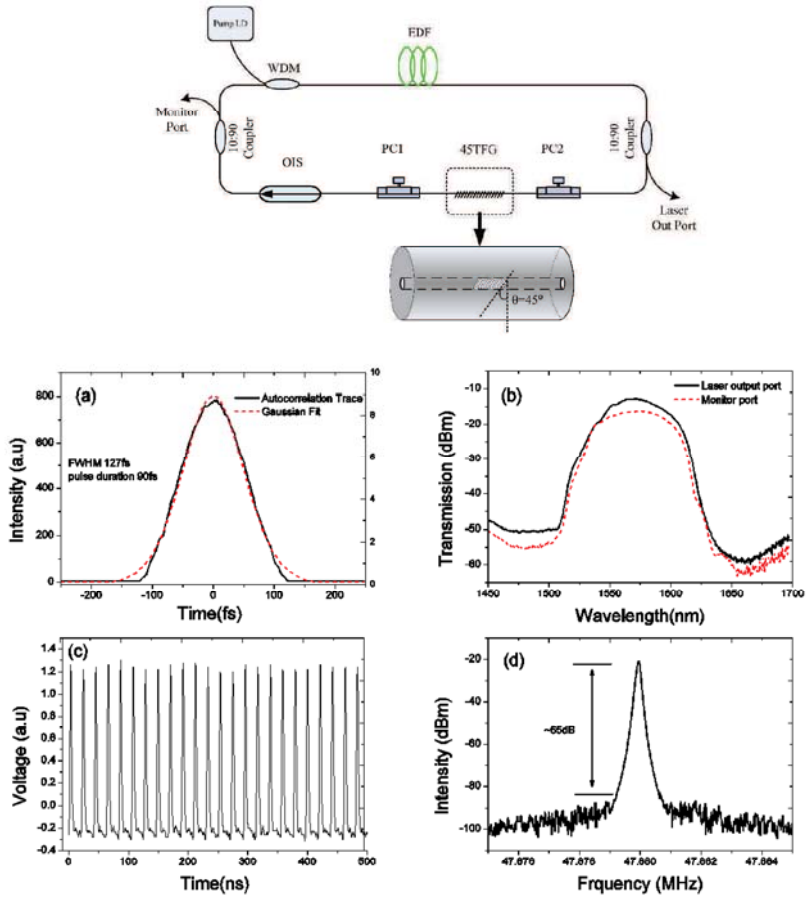

Fig. 10. Top: Schematic configuration of a 45°-TFG based mode-locked stretched-pulse fiber laser. Bottom: (a) Measured auto-correlation trace and corresponding Gaussian fit, (b) optical spectra of output and monitor ports, (c) typical output pulse train and (d) radio-frequency spectrum. Adapted from Ref. 69.

fiber gratings. Future studies will pursue the use of this all-fiber configuration in all-normal dispersion mode-locked fiber lasers[5] to achieve high pulse energies.

3.2. *Carbon nanomaterial based saturable absorbers*

Carbon nanomaterials such as CNTs and graphene[40,41,44] are promising saturable absorbers, at the center of a growing research effort due to their fast recovery times, broad operation range, low saturation intensity, low cost and easy fabrication. The first CNT mode-locked soliton fiber laser employed a free-space coupled CNT saturable absorber.[40,41] The later availability of CNT polymer composites has boosted the development of the field by enabling all-fiber structure soliton fiber lasers.[42] The CNT polymer saturable absorber can be attached to the end of a standard fiber

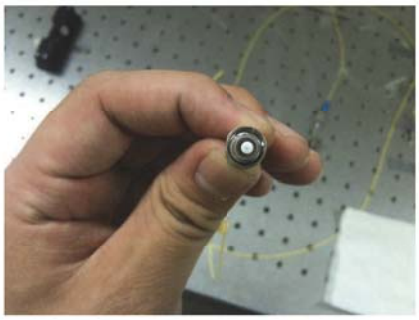

Fig. 11. A typical fiber based CNT saturable absorber.

ferrule (Fig. 11). Since then, various types of CNT polymer composites have been studied for CNT mode locker in fiber lasers.[72–75] Recently, CNTs were demonstrated as mode lockers for a stretched-pulse erbium-doped fiber laser generating pulses shorter than 100 fs.[76] By properly designing the cavity dispersion map, dissipative soliton generation from a CNT-based fiber laser was also demonstrated.[77] Similarly to CNTs, so far graphene polymer composites have been used to realize mode-locking soliton generation.[44,78]

4. Polarization Dynamics

4.1. *Experimental setup and methods*

In our experiment, we used a ring-cavity fiber laser similar to that shown in Fig. 1, which comprised a 2 m-long segment of high-concentration erbium-doped fiber, a single-mode fiber segment with anomalous dispersion, polarization controllers, a WDM coupler, an optical isolator, a fast (370 fs relaxation time) saturable absorber in the form of CNT-doped polymer film and an output coupler.[28,29] The total cavity length was 7.83 m. The cavity was pumped via 980/1550 WDM by a 976 nm laser diode with a maximum current of about 355 mA (170 mW optical power). The laser output was analyzed with the help of an optical spectrum analyzer and an inline polarimeter with the resolution 2 ns, and the number of samples was 10,000.[29] The polarimeter measured the normalized Stokes parameters s_1, s_2, s_3 and degree of polarization (DOP) which are related to the output powers of two linearly cross-polarized SOPs $|u|^2$ and $|v|^2$, and phase difference between them $\Delta\phi$ as follows:

$$\begin{gathered} S_0 = |u|^2 + |v|^2\,, \quad S_1 = |u|^2 - |v|^2\,, \\ S_2 = 2|u||v|\cos\Delta\phi\,, \quad S_3 = 2|u||v|\sin\Delta\phi\,, \\ s_i = \frac{S_i}{\sqrt{S_1^2+S_2^2+S_3^2}}\,, \quad \mathrm{DOP} = \frac{\sqrt{S_1^2+S_2^2+S_3^2}}{S_0}\,, \quad i = 1,2,3\,. \end{gathered} \tag{7}$$

The polarimeter consisted of four TFGs recorded in the core of a polarization-maintaining fiber (Fig. 12). Each grating acts as a 1% polarization sensitive tap

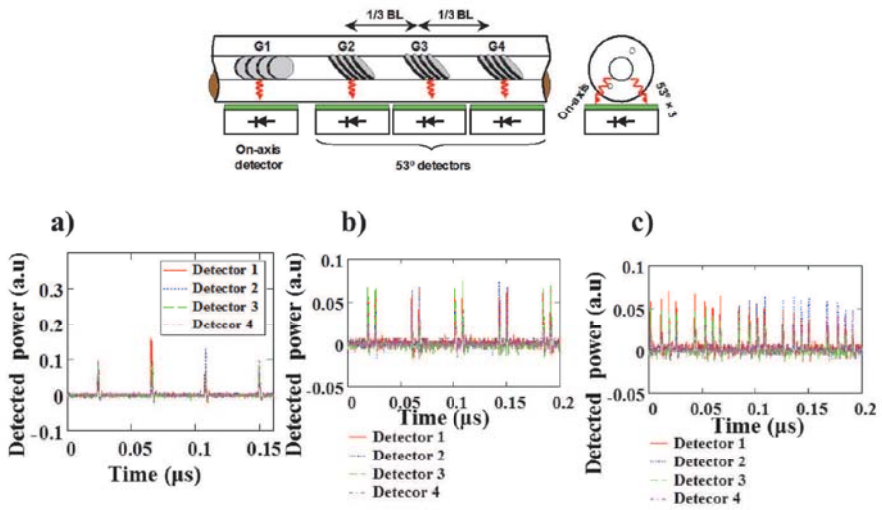

Fig. 12. Top: Schematic diagram of the polarimeter. Bottom: Pulse train collected by four polarimeter photodetectors for (a) bound state and (b) and (c) multi-pulse soliton operations. Adapted from Ref. 29.

which scatters the incoming light on the detector when its polarization is aligned with the grating orientation. Four detector voltages were recorded simultaneously using an oscilloscope. In order to relate the polarimeter detector voltages to the Stokes parameters, a 4×4 calibration matrix obtained by self-calibration procedure was used.[29] The data collected from the oscilloscope (Fig. 12) were filtered with an Hanning filter and the Stokes parameters were calculated for each laser pulse.[29]

4.2. *Tightly bound vector solitons — soliton molecules*

Bound-state solitons originate from a balance of repulsive and attractive forces between solitons caused by Kerr nonlinearity and dispersion, which can result in tightly bound states in terms of fixed and discrete pulse separation and phase differences of 0, π, or $\pm\pi/2$.[79,80] Tightly bound-state solitons have been experimentally observed in NPR, figure-of-eight, CNT and graphene based mode-locked fiber lasers.[81–87] In addition, various types of bound states have been studied theoretically and experimentally, including vibrating and oscillating bound states,[88] and bound states with flipping and independently evolving phase.[89] The pulse separation and phase difference of a bound-state soliton can be determined using optical spectra analysis. For a two-soliton bound state with the pulse separation τ and the phase shift ϕ, the amplitude is given by $f(t)+f(t+\tau)\exp(i\phi)$, and the corresponding optical spectrum can be presented as[87]

$$S(\omega) = 2|\hat{f}(\omega)|^2(1+\cos(\omega\tau-\phi))\,, \tag{8}$$

where $\hat{f}(\omega)$ is the Fourier transform of $f(t)$. Therefore, the optical spectrum is modulated with the frequency $\Delta\omega = 1/\tau$, the symmetry of the spectrum is phase-

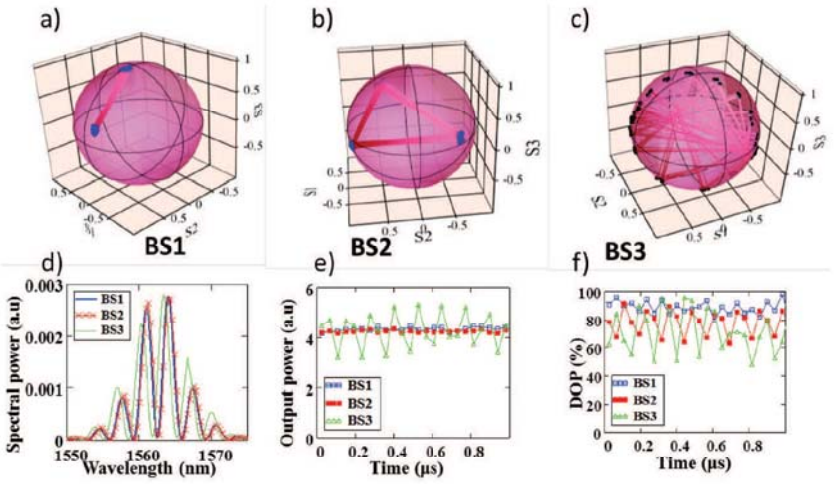

Fig. 13. Stokes parameters on the Poincaré sphere illustrating the polarization dynamics of bound-state solitons in the forms of polarization switching between (a) two and (b) three SOPs, and (c) superposition of polarization switching among three SOPs and SOP precession, (d) output optical spectrum, (e) power and (f) DOP for the bound states shown in (a)–(c). Adapted from Ref. 29.

shift dependent, and the spectral power at the points of minimum is close to zero. For mode-locked lasers with anomalous dispersion, the pulse has an hyperbolic-secant shape with a time-bandwidth product of 0.315. Thus, the pulse width T_p and pulse separation τ can be estimated from the optical spectrum as

$$T_p = \frac{0.315 n \lambda^2}{c \Delta\lambda}, \quad \tau = T_p / N, \tag{9}$$

where $n = 1.44$ is the refractive index of silica fiber, λ is the central wavelength of the spectrum, c is the speed of light and N the number of minima in the spectrum. The metrics above can be used to quantify soliton bound states.

In our experiment, the pump current was approximately 300 mA and the in-cavity polarization controller and the polarization controller for the pump laser were tuned to obtain the polarization attractors for bound-state soliton operations shown in Figs. 13(a)–13(c).[28,29] The polarization dynamics in Figs. 13(a) and 13(b) take the form of polarization switching between two and three SOPs with a period equaling two and three pulse round trips in the cavity, respectively. The corresponding output optical spectra [Fig. 13(d)] show both the presence of a bound state of two solitons with a fixed phase difference of $\phi = \pi$. The pulse width and pulse separation estimated from the spectra are $T_p = 370$ fs and $\tau = 1.5$ ps, indicating a tightly bound state ($\tau < 5T_p$). The total output power from the laser [Fig. 13(e)] is constant within ±5% precision, and DOP oscillations around the respective values of 90% and 80% are observed [Fig. 13(f)]. Because the detector integration time (2 ns) is longer than the pulse separation, these high DOP values indicate that the bound solitons have the same SOP. The DOP would otherwise be close to zero for

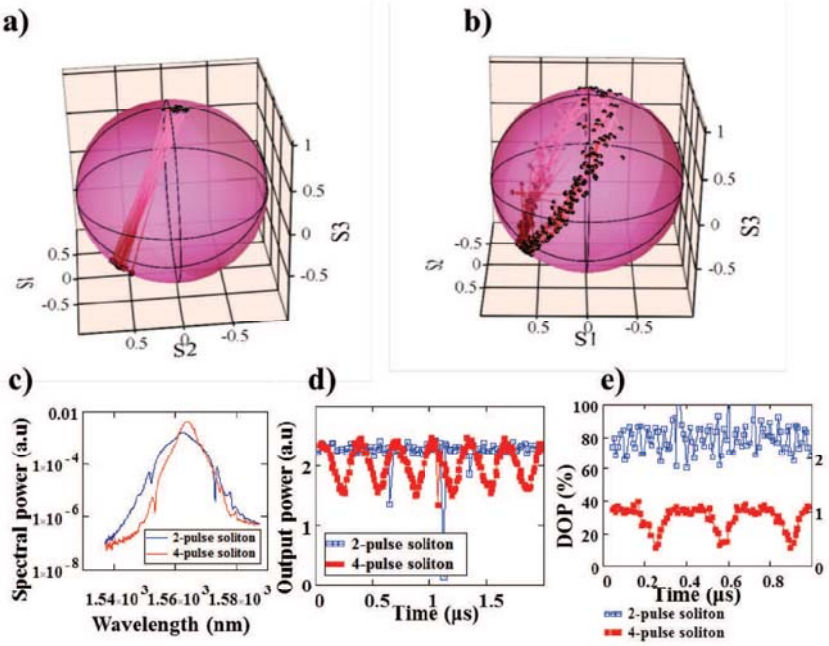

Fig. 14. Stokes parameters on the Poincaré sphere illustrating the polarization dynamics of (a) two-pulse and (b) four-pulse solitons, (c) output optical spectrum, (d) power and (e) DOP for the multi-pulse solitons is shown in (a) and (b).

orthogonal SOPs. The slight asymmetry of the spectra is likely due to a hopping between π- and $-\pi/2$-shifted bound states that arises from changing the erbium gain spectrum under long-term fluctuations of ambient temperature.[87] The high contrast of the spectral fringes and small asymmetry of the spectrum indicate that lifetime of the π-shifted bound state is much longer than that of the $-\pi/2$-shifted bound state. Otherwise, the spectrum takes the form shown in Fig. 13(d) for the bound state labeled "BS3", i.e., it is close to a $-\pi/2$-shifted tightly bound state with a pulse width of 370 fs and pulse separation of 1.5 ps. In this case, the SOP evolution takes the form of superposition of switching among three SOPs and precession of these SOPs along a circle trajectory on the Poincaré sphere with periods of three and twenty round trips, respectively [Fig. 13(c)]. The output power and DOP oscillate with these two periods [Figs. 13(e) and 13(f)].

4.3. *Multi-pulse vector solitons*

In addition to polarization attractors for bound-state operations, we have also observed polarization dynamics for two- and four-pulse soliton operations [Figs. 14(a) and 14(b)]. Though the spectrum features the typical shape of a fundamental soliton with Kelly sidebands [Fig. 14(c)], the oscilloscope reveals multi-pulse operation (Fig. 12). The observed multi-pulsing arises in the laser as a result of an interplay

between the bandwidth constraints of the laser cavity and the energy quantization associated with the resulting mode-locked pulses.[59] The polarization dynamics for the two-pulse soliton operation takes the form of polarization switching between cross-polarized SOPs with a period equaling the pulse round-trip time. Note that the SOP of the two pulses is preserved within one round trip. DOP oscillations around the value of 80% are observed [Fig. 14(e)]. The total laser power [Fig. 14(d)] is constant within ±5% precision. The polarization dynamics for the four-pulse soliton operation shows slow pulse-to-pulse evolution of the laser SOP with a period of 335 ns corresponding to eight round trips in the cavity. In contrast to the two-pulse case, the four-pulse vector soliton exhibits cyclic SOP evolution. The DOP value is approximately 1%, which indicates a fast SOP evolution inside the four-pulse bunch.

4.4. *Discussion*

As shown in Refs. 32 and 33, the eigenstates in a fiber in the presence of linear birefringence and circular birefringence caused by nonlinear SPM are split into two pairs:

$$S^{(1,2)} = \begin{pmatrix} S_0 \\ \pm S_0 \\ 0 \\ 0 \end{pmatrix}, \quad S^{(3,4)} = \begin{pmatrix} S_0 \\ \alpha \\ 0 \\ \pm\sqrt{S_0^2 - \alpha^2} \end{pmatrix}. \tag{10}$$

Here, $S_0 = \text{const}$ and α is determined by the ratio of linear to circular birefringence strength. In a mode-locked laser, the in-cavity polarization controller contributes to both linear and circular birefringence whereas the anisotropy induced by the pump light is suppressed due to orientation relaxation caused by excitation migration.[90] The mode-locked operation changes the active medium anisotropy (both linear and circular) due to polarization hole burning,[90,91] and the resulting pulse SOP is located on a circle. If the beat length in the anisotropic cavity is equal to the round trip distance and the pulse-to-pulse power is constant, then the pulse SOP is fixed and the resulting vector soliton is polarization locked.[19,20] For a round trip distance equaling one half or third of the beat length, the SOP is reproduced periodically every two or three round trips, and the polarization switching takes the forms shown in Figs. 13(a), 13(b) and 14(a). The depth of the hole in the orientation distribution of inversion is proportional to the laser power and, thus, the light induced anisotropy in the active medium will be periodically modulated with the periodical oscillations of the output power.[90,91] If the round trip is equal to a rational part of the beat length, then the SOP will slightly deviate from its initial state after a few round trips, and can only reproduce itself over the period of the pulse power oscillations [Figs. 13(c) and 14(b)].

5. Conclusion

We have provided an overview of several new nonlinear mechanisms of pulse shaping that currently drive rapid progress in passively mode-locked fiber lasers, as well as of the previously known soliton and DM soliton mode-locking regimes. Specifically, we have discussed passive and active similariton mode locking, a mode-locking regime featuring pulses with a triangular distribution of the intensity, and spectral compression arising from nonlinear pulse propagation. From a fundamental standpoint, the new pulse evolutions reviewed here open new possibilities for studying nonlinear dynamical processes. From a practical viewpoint, these regimes of pulse shaping are of particular relevance with the high interest in the generation of specialized pulse waveforms for applications in optical signal processing and manipulation.[92] In particular, the simple intensity profile of triangular pulses is desired for a range of processing applications, including time-domain add-drop multiplexing,[93,94] wavelength conversion,[95,96] and optical pulse doubling in frequency and time.[97] The ability to generate highly-chirped parabolic pulses and transform-limited spectrally compressed picosecond pulses from a single device is attractive for applications. In particular, narrow-spectrum pulses are desired in applications requiring high spectral resolution such as in nonlinear vibrational microscopy.

We have also discussed various experimental methods that are currently used and/or actively studied to realize mode-locking pulse generation in fiber lasers. These included the use of a 45°-TFG as an in-fiber polarizer in soliton and DM soliton lasers relying on NPR for mode locking, which could provide several advantages when compared to bulk polarizers, including low insertion loss, high stability and integrability, and the use of carbon nano-materials as saturable absorbers.

Further, we have reported on recent experimental findings on new types of vector soliton molecules and multi-pulse vector solitons in an anomalous-dispersion, CNT mode-locked fiber laser. The observation of these new polarization dynamics was made possible by the use of a specially designed inline polarimeter optimized for high-speed pulse-to-pulse SOP measurement operation. By unveiling the origin of new types of unique SOPs evolving on very complex trajectories, our experimental studies can find applications in the development of new laser designs with controlled dynamical SOPs, as well as in the context of increased capacity in fiber optic communications based on polarization-division multiplexing, polarization switched, and modified coded hybrid subcarrier/amplitude/phase/polarization modulation schemes.[30,31] Further, our results pave the way to new techniques in nano-optics (trapping and manipulation of nanoparticles and atoms)[24,25] and spintronics (vector control of magnetization).[26]

Acknowledgments

We acknowledge important contributions of our colleague, Dr. Alexei Rozhin into the original papers on CNT mode-locked fiber lasers. We would like also to acknowledge support by the Leverhulme Trust (grant RPG-278), the European Re-

search Council (project ULTRALASER), the Engineering and Physical Sciences Research Council (project UNLOC, EP/J017582/1), the European Commission (FP7-PEOPLE-2012 Industry-Academia Partnerships and Pathways, project GRIFFON, 324391) and the Ministry of Education and Science of the Russian Federation (grant agreement 14.B25.31.0003).

References

1. N. Akhmediev and A. Ankiewicz (eds.), *Dissipative Solitons, Lecture Notes in Physics*, Vol. 661 (Springer, Berlin, 2005).
2. I. N. Duling, *Electron. Lett.* **27**, 544 (1991).
3. K. Tamura, E. P. Ippen, H. A. Haus and L. E. Nelson, *Opt. Lett.* **18**, 1080 (1993).
4. S. K. Turitsyn, B. Bale and M. P. Fedoruk, *Phys. Rep.* **521**, 135 (2012).
5. W. H. Renninger, A. Chong and F. W. Wise, *IEEE J. Sel. Top. Quantum Electron.* **18**, 389 (2012).
6. W. H. Renninger, A. Chong and F. W. Wise, *Phys. Rev. A* **77**, 023814 (2008).
7. F. Ö. Ilday, J. R. Buckley, W. G. Clark and F. W. Wise, *Phys. Rev. Lett.* **92**, 213902 (2004).
8. B. Oktem, C. Ülgüdür and F. Ö. Ilday, *Nature Photon.* **4**, 307 (2010).
9. Z. X. Zhang, B. Oktem and F. Ö. Ilday, *Opt. Lett.* **37**, 3489 (2012).
10. W. H. Renninger, A. Chong and F. W. Wise, *Phys. Rev. A* **82**, 021805 (2010).
11. B. G. Bale and S. Wabnitz, *Opt. Lett.* **35**, 2466 (2010).
12. C. Aguergaray, D. M'echin, V. Kruglov and J. D. Harvey, *Opt. Express* **18**, 8680 (2010).
13. S. Boscolo and S. K. Turitsyn, *Phys. Rev. A* **85**, 043811 (2012).
14. S. Boscolo, S. K. Turitsyn and C. Finot, *Opt. Lett.* **37**, 4531 (2012).
15. B. C. Collings *et al.*, *J. Opt. Soc. Amer. B* **17**, 354 (2000).
16. H. Zhang, D. Y. Tang, L. M. Zhao and H. Y. Tam, *Opt. Lett.* **33**, 2317 (2008).
17. L. M. Zhao, D. Y. Tang, H. Zhang and X. Wu, *Opt. Express* **16**, 10053 (2008).
18. D. Y. Tang, H. Zhang, L. M. Zhao and X. Wu, *Phys. Rev. Lett.* **101**, 153904 (2008).
19. C. Mou, S. V. Sergeyev, A. Rozhin and S. K. Turitsyn, *Opt. Lett.* **36**, 3831 (2011).
20. S. V. Sergeyev, C. Mou, A. Rozhin and S. K. Turitsyn, *Opt. Express* **20**, 27434 (2012).
21. T. Udem, R. Holzwarth and T. W. Hänsch, *Nature* **416**, 233 (2002).
22. J. Mandon, G. Guelachvili and N. Picqué, *Nature Photon.* **25**, 99 (2009).
23. D. Hillerkuss *et al.*, *Nature Photon.* **5**, 364 (2011).
24. Y. Jiang, T. Narushima and H. Okamoto, *Nature Phys.* **6**, 1005 (2010).
25. L. Tong, V. D. Miljkovic and M. Käll, *Nano Lett.* **10**, 268 (2010).
26. N. Kanda *et al.*, *Nature Commun.* Doi:10.1038/ncoms1366 (2011).
27. G. D. Van Wiggeren and R. Roy, *Phys. Rev. Lett.* **88**, 097903 (2002).
28. C. Mou, S. V. Sergeyev, A. Rozhin and S. K. Turitsyn, *Opt. Express* **21**, 26868 (2013).
29. V. Tsatourian *et al.*, *Sci. Rep.* (2013), doi:10.1038/srep03154
30. P. Serena, N. Rossi and A. Bononi, *Opt. Express* **20**, 7895 (2012).
31. H. G. Batshon *et al.*, *Opt. Express* **18**, 14108 (2010).
32. N. Akhmediev and J. M. Soto-Crespo, *Phys. Rev. E* **49**, 5742 (1994).
33. A. Komarov *et al.*, *Phys. Rev. A* **82**, 013813 (2010).
34. H. A. Haus, *IEEE J. Sel. Top. Quantum Electron.* **6**, 1173 (2000).
35. G. P. Agrawal, *Nonlinear Fiber Optics* (Academic Press, New York, 2007).
36. K. Tamura, H. A. Haus and E. P. Ippen, *Electron. Lett.* **28**, 2226 (1992).
37. H. A. Haus *et al.*, *IEEE J. Quantum Electron.* **31**, 591 (1995).
38. U. Keller, *Nature* **424**, 831 (2003).

39. O. Okhotnikov, A. Grudinin and M. Pessa, *New J. Phys.* **6**, 177 (2004).
40. S. Y. Set *et al.*, *IEEE J. Sel. Top. Quantum Electron.* **10**, 137 (2004).
41. S. Y. Set *et al.*, *J. Lightwave Technol.* **22**, 51 (2004).
42. A. G. Rozhin *et al.*, *Appl. Phys. Lett.* **88**, 051118 (2006).
43. F. Wang *et al.*, *Nature Nanotechnol.* **3**, 738 (2008).
44. H. Zhang *et al.*, *Appl. Phys. Lett.* **95**, 141103 (2009).
45. B. Bale, O. G. Okhotnikov and S. K. Turitsyn, in *Fiber Lasers*, ed. O. G. Okhotnikov (Wiley-VCH, Berlin, 2012).
46. S. K. Turitsyn *et al.*, *CR Phys. Acad Sci.* **4**, 145 (2003).
47. N. J. Smith *et al.*, *J. Lightwave Technol.* **15**, 1808 (1997).
48. I. Gabitov and S. K. Turitsyn, *Opt. Lett.* **21**, 327 (1996).
49. F. W. Wise, A. Chong and W. H. Renninger, *Laser Photon. Rev.* **2**, 58 (2008).
50. D. Anderson *et al.*, *J. Opt. Soc. Amer. B* **9**, 1358 (1992).
51. D. Anderson *et al.*, *J. Opt. Soc. Amer. B* **10**, 1185 (1993).
52. M. E. Fermann *et al.*, *Phys. Rev. Lett.* **84**, 6010 (2000).
53. V. I. Kruglov *et al.*, *J. Opt. Soc. Amer. B* **19**, 461 (2002).
54. J. M. Dudley *et al.*, *Nature Phys.* **3**, 597 (2007).
55. S. Boscolo, A. I. Latkin and S. K. Turitsyn, *IEEE J. Quantum Electron.* **44**, 1196 (2008).
56. G. I. Barenblatt, *Scaling, Self-Similarity and Intermediate Asymptotics* (Cambridge University Press, Cambridge, 1996).
57. H. Wang *et al.*, *J. Opt.* **12**, 035205 (2010).
58. S. A. Planas *et al.*, *Opt. Lett.* **18**, 699 (1993).
59. F. Li, P. K. A. Wai and J. N. Kutz, *J. Opt. Soc. Amer. B* **27**, 2068 (2010).
60. K. O. Hill *et al.*, *Appl. Phys. Lett.* **32**, 647 (1978).
61. B. S. Kawasaki *et al.*, *Opt. Lett.* **3**, 66 (1978).
62. J. Canning and M. G. Sceats, *Electron. Lett.* **30**, 1344 (1994).
63. S. W. James and R. P. Tatam, *Meas. Sci. Technol.* **14**, R49 (2003).
64. X. W. Shu *et al.*, *Opt. Lett.* **26**, 774 (2001).
65. T. Erdogan and J. E. Sipe, *J. Opt. Soc. Amer. A* **13**, 296 (1996).
66. C. Mou *et al.*, *Opt. Express* **18**, 18906 (2010).
67. Z. J. Yan *et al.*, *Opt. Lett.* **37**, 4522 (2012).
68. X. L. Liu *et al.*, *Opt. Express* **20**, 19000 (2012).
69. Z. Zhang *et al.*, *Opt. Express* **21**, 28297 (2013).
70. K. M. Zhou *et al.*, *Opt. Lett.* **30**, 1285 (2005).
71. Z. J. Yan *et al.*, *J. Lightwave Technol.* **29**, 2715 (2011).
72. A. Martinez *et al.*, *Opt. Express* **16**, 11337 (2008).
73. F. Shohda *et al.*, *Opt. Express* **16**, 20943 (2008).
74. T. Hasan *et al.*, *Adv. Mater.* **21**, 3874 (2009).
75. F. Shohda *et al.*, *Opt. Express* **18**, 11223 (2010).
76. D. Popa *et al.*, *Appl. Phys. Lett.* **101**, 153107 (2012).
77. J. H. Im *et al.*, *Opt. Express* **18**, 22141 (2010).
78. D. Popa *et al.*, *Appl. Phys. Lett.* **97**, 203106 (2010).
79. B. A. Malomed, *Phys. Rev. A* **44**, 6954 (1991).
80. N. N. Akhmediev, A. Ankiewicz and J. M. Soto-Crespo, *Phys. Rev. Lett.* **79**, 4047 (1997).
81. P. Grelu *et al.*, *Opt. Lett.* **27**, 966 (2002).
82. N. H. Seong and D. Y. Kim, *Opt. Lett.* **27**, 1321 (2002).
83. D. Y. Tang *et al.*, *Phys. Rev. E* **72**, 016616 (2005).
84. B. Zhao *et al.*, *Phys. Rev. E* **70**, 067602 (2004).

85. X. Wu *et al.*, *Opt. Commun.* **284**, 3615 (2011).
86. X. L. Li *et al.*, *Laser Phys.* **22**, 774 (2012).
87. L. L. Gui, X. S. Xiao and C. X. Yang, *J. Opt. Soc. Amer. B* **30**, 158 (2013).
88. P. Grelu and N. N. Akhmediev, *Nature Photon.* **26**, 84 (2012).
89. A. Zavyalov *et al.*, *Phys. Rev. A* **80**, 043829 (2009).
90. S. V. Sergeyev, *Phys. Rev. A* **59**, 3909 (1999).
91. H. Zeghlache and A. Boulnois, *Phys. Rev. A* **52**, 4229 (1995).
92. S. Boscolo and C. Finot, *Intern. J. Opt.* **2012**, (2012).
93. J. Li *et al.*, *J. Lightwave Technol.* **23**, 2654 (2005).
94. F. Parmigiani *et al.*, *Opt. Express* **17**, 8362 (2009).
95. F. Parmigiani *et al.*, *IEEE Photon. Technol. Lett.* **21**, 1837 (2009).
96. N. Verscheure and C. Finot, *Electron. Lett.* **47**, 1194 (2011).
97. A. I. Latkin *et al.*, *J. Opt. Soc. Amer. B* **26**, 1492 (2009).